JOURNAL OF SOLID STATE CHEMISTRY 88, 8–27 (1990)

Systematics in Band Gaps and Optical Spectra of 3D Transition Metal Compounds

J. ZAANEN[1] AND G. A. SAWATZKY

Laboratory of Applied and Solid State Physics, Materials Science Centre, University of Groningen, Nijenborgh 18, 9747 AG Groningen, The Netherlands

Received May 24, 1990

DEDICATED TO J. M. HONIG ON THE OCCASION OF HIS 65TH BIRTHDAY

In this paper we discuss the systematics in the transition metal d–d Coulomb interactions and the anion to cation charge transfer energies, and relate these to systematics in observed band gaps. In addition, we discuss the nature of the optical thresholds and their dependence on the cation and anion electronegativity. © 1990 Academic Press, Inc.

The discovery of the high T_c superconductors (*1*), in which cupric oxide planes play an important role, has once again revived long standing questions regarding the importance of correlation effects in understanding the electronic structure of transition metal (TM) compounds. Already in 1937 it was pointed out by de Boer and Verwey (*2*) that the insulating late (Mn–Cu) 3*d* TM compounds contradict the predictions of the one-electron theory of solids presented by Bloch (*3*) and Wilson (*4*). Mott (*5*) and Hubbard (*6*) provided a basic solution to this problem by pointing out that a one-electron description of solids is expected to break down if the Coulomb and exchange energies (U) involved in charge fluctuations of the type $d_i^n d_j^n \rightarrow d_i^{n-1} d_j^{n+1}$ (where i and j label sites and n the d orbital occupation) are large compared to the one-electron dispersional band width (w). For $U \gg w$ polarity fluctuations as above are suppressed, and a correlation gap of order U occurs in the excitation spectrum. This idea of suppressed charge fluctuations has formed the basis for an understanding of the low-energy scale properties of magnetic insulators in terms of spin-only Hamiltonians, the success of which confirms that charge fluctuations must be high-energy-scale properties. This separation into low (spin only)- and high (charge fluctuations)-energy scales also forms the basis for the very successful Anderson (*7*) theory of superexchange and the related Goodenough–Kanamori rules (*8*). These ideas and theoretical work by Gutzwiller (*9*) and Brinkman and Rice (*10*) have helped us tremendously in understanding the properties including the composition dependence of the early (Ti–Cr) TM compounds (*11*) which exhibit a very rich phase diagram including metallic, paramagnetic insulating and antiferromagnetic insulating regions.

[1] Present address: Max Planck Institut, Postfach 800665, D-7000 Stuttgart 80, FRG.

0022-4596/90 $3.00

The Mott–Hubbard basic picture however runs into some trouble for the late (Mn–Cu) TM compounds if one considers the systematics of band gaps or anion electronegativity (*12*) as, for example, in NiF_2, $NiCl_2$, $NiBr_2$, and NiI_2 (*13*). These observations together with the description of Raman (*14*) as well as optical and transport data (*15, 16*) suggest a breakdown of the Mott–Hubbard picture for the late TM compounds in which the lowest energy charge fluctuation excitations involve only d states and U. Photo and inverse photoemission data on NiO and $NiCl_2$ were more recently also shown to be inconsistent with a simple Mott–Hubbard picture (*17, 18*) and it was suggested that the band gap was not of a d–d type but rather of a O $2p$–Ni $3d$ charge transfer type. This is a rather important conclusion because formerly the charge transfer states were included in theories involving superexchange and transferred hyperfine interactions with the assumption that the charge transfer energy Δ was very large ($\Delta \gg U$) and therefore the influence of these states could be incorporated via somewhat more delocalized TM $3d$ orbitals. This leads directly to an effective TM $3d$–TM $3d$ interatomic hopping integral given by t_{pd}^2/Δ and a resulting superexchange interaction of $J_{\text{sup}} = 2(t_{pd}^4)/(\Delta^2)(1/U)$ where t_{pd} is the TM $3d$ anion $2p$ transfer integral. As shown recently (*19*) by explicitly including the charge transfer states in the theory the superexchange interaction is modified to $J_{\text{sup}} = (2t_{pd}^4)/(\Delta^2)[(1/U) + (1/\Delta)]$ which includes explicitly the excited states with two holes on the intervening anion. The anion on site p–p Coulomb repulsion (U_{pp}) can be included by replacing Δ by $\Delta + (U_{pp}/2)$ (20). The most important point however is that if the gap is a charge transfer gap, then the first ionization state is not one involving a TM $3d$ state but one involving an anion p state. This is important because in this case the charge compensating holes in, for example, $La_{2-x}Sr_xCuO_4$ of $Li_xNi_{1-x}O$ would not lead to respectively Cu^{3+} and Ni^{3+} but to holes in the O $2p$ band as is now known to be the case (*21, 22*)

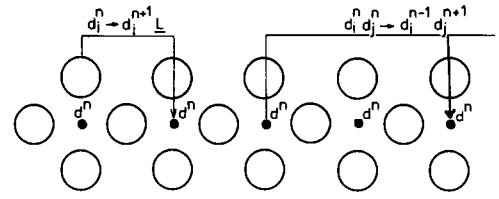

FIG. 1. Representation of an ionic lattice consisting of TM ions (d^n) and closed shell anions. The most important charge fluctuation excitations are indicated.

The question we want to address in this paper is how do U, Δ, and TM $4s,p$ band edge vary with TM ion, anion and crystal structure and what is the role of covalency in all this. To do this we briefly review the basic concepts of an approach to this problem introduced by us in 1984–1985 (*23, 24*). We then use both experimental and theoretical estimates of the relevant parameters to describe the cation and anion as well as the structural dependence of these. We end up with some predictions concerning the optical properties and the influence of doping.

Basic Model

Since the basic model (*23, 24*) has been reviewed several times (*19, 20, 25*) we restrict ourselves to a very brief description in order to define the problem. A commonly accepted basis for discussion of the electronic structure of TM compounds is the ionic model. This is illustrated in Fig. 1. In the ionic ground state, each TM metal ion is in a d^n configuration and the anions have a closed shell p^6 configuration. For $10 > n > 0$, each TM ion has internal degrees of freedom corresponding to the various spin and orbital arrangements of the n electrons. The lowest energy configuration for high spin compounds is that dictated by Hund's rule. There are, however, many excited-

state configurations within d^n whose energies are determined by the Racah parameters and the crystal-field splittings (*26*). These states can range over energies of about 10 eV and their energies and symmetries can be found from the Tanabe–Sugano (*27*) diagrams. The excited states do not contribute to the electrical conductivity because charge fluctuations are not involved. They do, however, contribute to the optical properties often in the form of weak, sharp peaks appearing inside the band gap (*26*).

In Fig. 1 we also show some of the possible excited states involving charge fluctuations. Basically there are four types that are important whose energies are given by

$$\Delta = E(|d^{n+1}(\underline{IR_0})\underline{L}>) - E(|d^n(IR_0)>) \quad (1)$$

$$U_{\text{eff}} = E(|d^{n+1}(IR_0)>) + E(|d^{n-1}(IR_0)>) - 2E(|d^n(IR_0)>) \quad (2)$$

$$\Delta_{\text{it}} = E(|d^n(IR_0)\underline{L}>) + E(|d^n(IR_0)s>) - 2E(|d^n(IR_0)>), \quad (3)$$

where $E(|d^x(IR_0)>)$ is the energy of the Hund's rule ground state term of the $3d^x$ configurations and $\underline{L}$ denotes a hole at the center of the ligand band (with width W) and s denotes an electron at the bottom of the conduction band. The fourth energy involving a d–$4s$ excitation is given by $U_{\text{eff}} - \Delta + \Delta_{\text{it}}$.

Even in the ionic picture there are two other quantities, the d band dispersional width (w) and the anion p band dispersional width (W), which are important for the excited states. The states $d_i^{n-1}d_j^{n+1}$, in fact, have a dispersional width of $\approx 2w$ and the excited states $d^{n+1}\underline{L}_k$ will have a dispersional width of $\approx W + w$ because of translational symmetry.

We are now in a position to draw a total-energy diagram based on the ionic ansatz as shown in Fig. 2 for $U \gg w$, $U > \Delta$, $\Delta > W$. In Fig. 2 we can see the various types of band gaps that might occur. For $U > \Delta$,

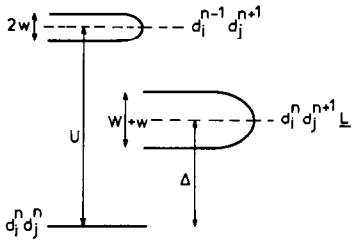

FIG. 2. Total energy level diagram corresponding to an ionic ground state and excitations as indicated in Fig. 1.

the gap is of a charge-transfer type and its magnitude is Δ-$W/2$. So even for $U \to \infty$ we can get a metallic ground state if $\Delta < W/2$. Because generally $w \ll W$, these materials are p-type metals as, for example, in CuS (*28*). For $\Delta > W/2$ the gap scales as the anion electronegativity for a given cation and crystal structure. This is the case for the series $NiCl_2$, $NiBr_2$, and NiI with gaps of 4.7, 3.5, and 1.7 eV respectively (*13*) and the closing of the gap for NiS.

For $U < \Delta$, we are in the Mott–Hubbard regime with a d–d gap for $U > w$ and a d band metal for $U < w$. It is generally accepted that the early $3d$ transition-metal oxides belong to this regime.

We can put all of this information into a simple phase diagram shown in Fig. 3 which is a simplified version of the diagram including hybridization recently presented by us (*23*).

To discuss covalency effects, we must include the hybridization between the various configurations shown in Figs. 1 and 2. A rigorous solution of this problem would involve solving the Anderson lattice Hamiltonian, which is, as yet, an impossible task. We can however, make a few approximations that are expected to be valid for the late $3d$ TM compounds. One possibility is to use one or the other strong coupling mean field approximation. Recently, it was shown that especially the Gutzwiller mean field theory gives quite reasonable results (*29*) How-

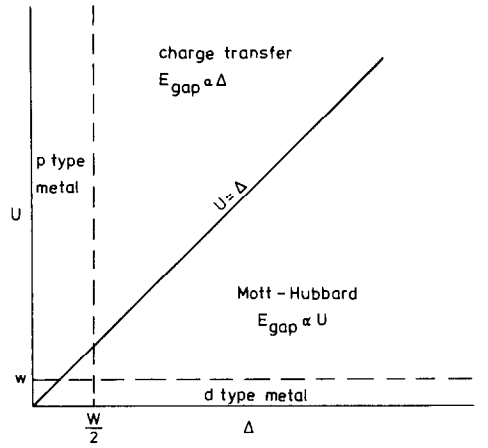

FIG. 3. Simple phase diagram showing the various types of insulating and metallic states in transition metal compounds.

ever, one should keep in mind that this approximation, although excellent for local properties, is somewhat uncontrolled in so far as collective properties like spin fluctuations and quasiparticle bandwidths are involved. On the other hand, from density functional band-structure calculations, it is found that the d band dispersional width of the monoxides is less than 0.5 eV (*30*) ($w <$ 0.5 eV). If we set $w = 0$, the Anderson lattice Hamiltonian becomes the Anderson impurity Hamiltonian. Even this is a formidable problem to solve for the metallic systems, leading to the Kondo, mixed valent, valence fluctuation, and spin fluctuation behavior. However, for insulators and with the neglect of the TM 4s band, the problem is relatively simple because it involves the solution of a system with a finite number of particles. The details of how to do this are described in Zaanen's thesis (*31*). The qualitative results for the states with one electron removed (photoemission spectra (PES)) and one electron added (the inverse photoemission spectrum (IPES) are shown in Fig. 4 for various scenarios: the dashed lines in each case represent what happens if we switch on the anion p-transition metal d hybridization.

The basic problem consists of treating a correlated impurity in a host which is described by a valence band (L) and a conduction band 4s with a gap given by $\Delta_{it} - W/2$. For a zero gap we basically have the Kondo problem shown in Fig. 4A. Also shown here are the multiplet splittings of the d^{n-1} and d^{n+1} configurations. Hybridization here results in a virtual bound state broadening and the possible formation of a Kondo resonance at the Fermi level. These states are observed in PES–IPES of rare earth metals by Lang *et al.* (*32*), Mn impurities in Ag by van der Marel *et al.* (*56*) and the Kondo resonance has recently been observed in PES by Schneider and Baer (*33*). We emphasize this here because the TM insulators and the Kondo problem are treated here in the same way with the difference being only, in the "host" band structure.

For the TM compounds the host is a semiconductor with a gap $\Delta_{it} - W/2$. We have four different possibilities which, depending on the size of U, Δ, and Δ_{it} correspond to a final gap of Tm d–TM d (Mott–Hubbard),

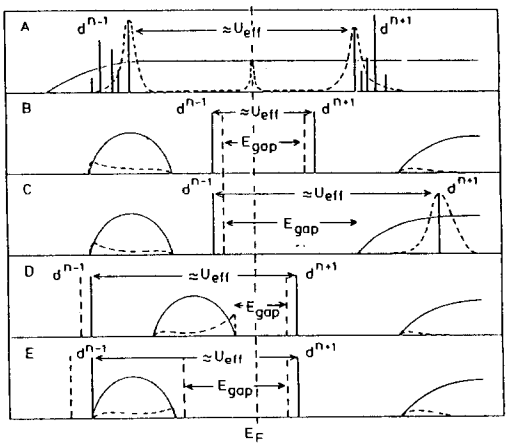

FIG. 4. An artist's concept of the possible situations encountered for strongly correlated impurities in solids. Dashed lines indicate the effect of hybridization.

TM d–TM $4s$, anion p–TM d (charge transfer), or even anion p–TM $4s$ ($\Delta_{it} - W/2$) character. A rather interesting case is shown in Fig. 4D in which the gap is basically of a charge transfer type but because of the strong hybridization between the d^{n-1} state and the anion p band a bound state can be pushed out of the top of the band. This new state now forms the first ionization state of the material. This situation looks much like that encountered in multiple charged impurities in semiconductors as described by Haldane and Anderson (*34*). This state has the symmetry and spin of the d^{n-1} configuration but the extra charge is primarily on the anion. For the case of NiO this state behaves magnetically and optically as if it were a $Ni^{3+}(3d^7)$ state (low spin ^2E) but in fact it is a state of primarily $d^8\underline{L}$ character with antiparallel spin and E symmetry, i.e., $d^8\underline{L}$ (^2E).

There are two rather interesting situations which can occur with regard to this bound state. First of all if the d^{n-1} state is higher in energy than the $d^n\underline{L}$ state ($U > \Delta$) then it is much easier to obtain a lowest energy bound state of low rather than high total spin. This was pointed out by Eskes *et al.* (*35*) and was shown by Eskes and Sawatzky (*36*) to be the probable reason for the stability of the Zhang–Rice singlet (*37*) in the high T_c materials. We reproduce in Fig. 5 the basis of the argument given by Eskes *et al.* (*35*). Drawn here are the energy levels for a Cu^{2+} impurity in say CuO. The ionization states are either $Cu^{3+}(d^8)$ or $Cu^{2+}O^-$ ($d^9\underline{L}$) as drawn. Also drawn are two of the many possible d^8 configurations in square planar symmetry, namely the high spin $^3B_{1g}(d^{\uparrow}_{x^2-y^2}, d^{\uparrow}_{3z^2-r^2})$ and the low spin $^1A_{1g}(d^{\uparrow}_{x^2-y^2}), d^{\downarrow}_{x^2-y^2})$ states. These are split by the d–d Racah parameters with a splitting of about 3.5 eV. We now switch on the d^8–$d^9\underline{L}$ hybridization which in square planar coordination is $\sqrt{3}$ times as strong for $x^2 - y^2$ orbitals than for $d_{3z^2-r^2}$ orbitals. For $U < \Delta$ (top two panels) the $d^8(^1A_{1g})$ state moves towards E_F more rapidly with t_{pd} than does the $^3B_{1g}$ state but a large t_{pd} is required before we get a high spin $\rightarrow$ low spin transition. However, for $U > \Delta$ the first bound state to appear is in fact the $^1A_{1g}$ state even for reasonable values of t_{pd}.

If we replace the $d^9\underline{L}$ band with single states of total $^3B_{1g}$ and $^1A_{1g}$ symmetry which are degenerate for no hybridization it is simple in perturbation theory to calculate the t_{pd} required for the high spin to low spin transition for $U \ll \Delta$,

$$\frac{t_{pd}^2}{\Delta - U} - \frac{1}{3}\frac{t_{pd}^2}{\Delta - U + J} > J, \tag{4}$$

where J is the Hund's rule splitting of $^3B_{1g}$ and $^1A_{1g}$ state. For $\Delta - U \gg t_{pd}, J$ we get the condition

$$\frac{t_{pd}^2}{\Delta - U} > \frac{3J}{2}, \tag{5}$$

whereas for $U \gg \Delta$ the low spin is the lowest if

$$\frac{t_{pd}^2}{U - \Delta} > \frac{t_{pd}^2}{3(U - \Delta - J)}; \tag{6}$$

so a low spin lowest energy state results for all t_{pd} if $U - \Delta > (3/2)J$. We emphasize this point here because it is a much more common occurring situation than only for the high T_cs. For the high T_cs Eskes and Sawatzky (*36*) have calculated a phase diagram which shows when the low or high spin case is the favorable one also for finite O $2p$ band widths.

The second rather interesting situation is if the d^{n-1} state hybridizes strongly with the valence band so that the bound state is pushed out well into the gap and the same occurs for the d^{n+1} state with the conduction band where a bound state is again pushed well into the gap. There is a point at which these bound states cross as we switch on the hybridization. This results in a strange situation in which U is effectively negative (attractive). The end result will be a valence dispro-

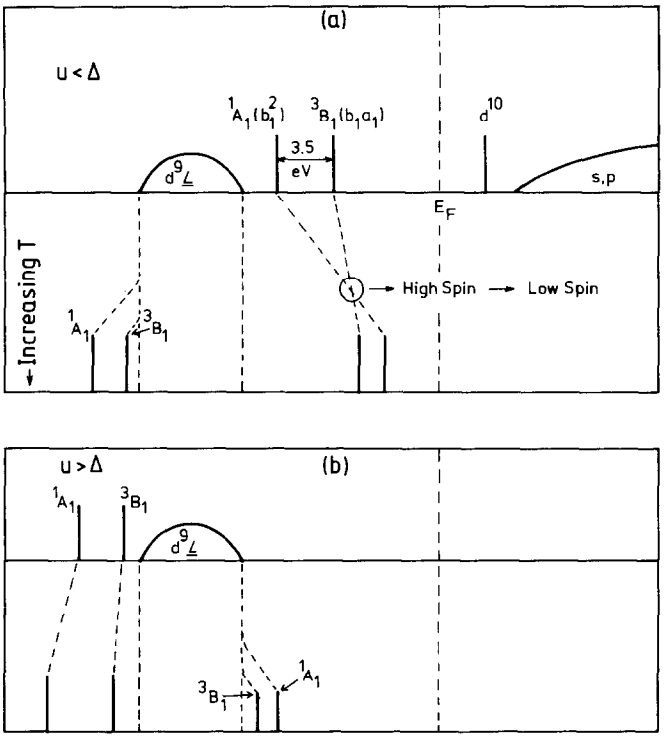

FIG. 5. An artist's concept of the shifts and changes occurring in the first ionized states of square planar coordinated Cu^{2+} as we switch on the Cu d–O p transfer integral for the two situations $U < \Delta$ and $U > \Delta$.

portionation into a ground state which looks like say $Cu^{3+} + Cu^{1+}$ rather than 2 Cu^{2+}. Such a disproportionation has been proposed for Cr impurities in Si (*38*). We should point out that the actual charge density for the examples above on the TM ions will remain close to those of the original ansatz.

Parameter Estimates

Returning to the phase diagram of Fig. 3 we now have ample evidence that NiO and CuO belong to the charge transfer class and Ti and V oxides to the Mott–Hubbard class. In order to discuss the systematics as a function of TM ion, anion, and structure it is useful to try to estimate the parameters of the above discussion.

These parameters are highly effective. For free atoms the parameters could be obtained from atomic ionization energies and electron affinities. In a solid, a number of additional interactions enter which are not considered explicitly in the impurity model. The philosophy is that these correspond to very fast processes compared to the time scale of interest. They dress the charge transfer and polarity fluctuations instantaneously and hence should lead to a simple renormalization of the parameters. The most important of these interactions are the Madelung energy, which stabilizes the ionic ground states in the insulators, the polarization energies, and the covalent effects arising from the mixing of the anion and cation s, p states. It is very difficult, if not impossi-

ble, to derive absolute magnitudes for the parameters on the basis of simple arguments. This is for instance reminiscent of the work of Adler and Feinlieb (*16*) and Koiller and Falicov (*15*) who arrived at the wrong conclusion that the conduction gap in the 3*d* compounds would be always of *d–s* character by using first principle estimates for the parameters.

The new development is the coming of the high energy spectroscopies. These data can be understood on the basis of the impurity model as shown by Zaanen (*30*) and empirical estimates for the parameters can be derived. In this way we have obtained parameters for NiO and the Ni–dihalides (*19*). Although the absolute magnitude of the parameters and also the variation with the ligand is difficult to estimate on theoretical grounds, the variation of the parameters as a function of 3*d* ion (keeping the ligand fixed) is easier to establish. Basically because the lattice parameter varies only slightly with the cation it is expected that the solid state corrections are roughly constant so that the parameters follow the trends of the atomic ionization energies of the cations. Using the empirical parameters found for Ni compounds as reference points, we present a rough outline of the systematics of the electronic structure of the 3*d* compounds as a function of cation and anion.

The strongest indication in favor of the validity of this procedure comes from optical spectroscopy, especially from work on 3*d* impurities in insulating hosts by McClure and co-workers (*39, 40*). Using data collected for the dichlorides (*41*) we show that the energetics suggest that in the concentrated systems interimpurity transitions can be identified, which confirms earlier suggestions (*42–43*).

The classical way to think about 3*d* insulators is to assume that these are highly ionic materials which are kept together by Madelung energies. Under the assumption that the itinerant gap is large compared to the energy scale of our interest, Δ and U are in this case determined by

$$\Delta^i = 2E^i_{\text{mad}}(M^{2+}X^{2-}) - E^i_I - E^i_A - E^i_{\text{pol}} \tag{7}$$

$$U^i = U^i(\text{at}) - 2E^i_{\text{pol}}, \tag{8}$$

where the superscript i refers to the ionic approximation and E^i_I is the ionization potential of M^{1+} and E^i_A is the electron affinity of O^{1-}. Here we see that the screening of the on-site Coulomb interaction U has a completely different form from the usual U/ε where ε is the long wavelength dielectric constant. This latter form is valid for describing the screening of an interaction between charges which are separated by more than several lattice constants. To obtain Eq. (8) consider the energy it costs to create a positive charge in a dielectric medium. This is given by $E_1 = E_I - E_{\text{pol}}$ and to have two charges well separated it is $2E_1 = 2E_I - 2E_{\text{pol}}$ but the energy required to create two charges on the same atom is $E_2 = 2E_I + U - 4E_{\text{pol}}$ assuming linear response. The reason for the factor of 4 is that the polarization energy goes as the charge squared because the one charge interacts with its own polarization cloud plus with that produced by the other charge. For a purely ionic compound

$$E_{\text{pol}} = \frac{1}{2}\sum_j \alpha_j F_j^2, \tag{9}$$

where F_j is the electric field of the point charge at ion j and α_j is the polarizability of ion j. According to de Boer *et al.* (*44*) $E_p \approx$ 3 eV in the monoxides and is proportional to $1/R^4$ where R is the interatomic distance.

Δ is a more complicated quantity, because it involves the energies $E(M^{2+}) - E(M^{1+}) = E_I$ as well as $E(O^{2-}) - E(O^-) = E_A$, the connection due to E_{pol}, as well as a large Madelung potential term ($2E_{\text{mad}}$).

Working this out for NiO, using the

known Madelung energy (~24 eV) and the standard estimate for $E_A = 9$ eV, we find that the Racah A (i.e., the monopole part of U) $A^i = 11.8$ eV and $\Delta^i = 17.8$ eV. The best estimates for A and Δ are probably derived from fitting the photoemission/inverse photoemmission spectra. We found (*31*) $A \approx \Delta \approx 6$ eV. Hence, this model overestimates U by a factor of two and Δ by a factor of three! In the past, this way of modeling has led to gross errors in the assignment of the excitation energies for the TMCs (*15, 16*).

Another approach is to use band structure calculations. There is no doubt that LDA bandstructure calculations are accurate with respect to the gross features of the charge distribution. Considering these results (*45*), the problem with the above is obvious: in reality the TMCs are much less ionic. The reason is that the ligand p orbitals hybridize quite strongly with the TM 4s electrons, leading to a significant occupancy of the latter, and the Wigner–Seitz spheres are in fact rather close to charge neutrality. Typically one finds charge separation of at most $\approx 1e$ (in the fluorides). In the Born–Maier framework one can mimic this by considering d^n4s^1, $d^{n+1}4s^1$, etc., configurations on the TM ions. Repeating the calculation for this $TM^{1+}L^{1-}$ scenario one finds that the Racah A (A^s) in NiO is now 8.9 eV, smaller than A^i because of the static screening of the 4s electron. Δ is more drastically reduced, because the Madelung energy gets smaller by a factor of four: we find now $\Delta^s = 12.2$ eV, assuming that the first electron affinity of O is zero. Although these numbers are significantly closer to experiment, they are still too large.

Apparently it is not possible to arrive at absolute estimates, using these simple considerations. It is instructive to consider the outcome of constrained LDA calculations (*46*), which have been shown to give quite accurate values for the parameters (*47–49*). In the study of the screening of U of a Mn impurity in different semiconducting hosts by Gunnarsson *et al.* (*50*), the different contributions to the screening are separated by applying several additional constraints to the system (*51*). Except for the polarization and the influence of s/p charge two additional effects are of importance. First, due to the boundary conditions the TM orbitals are somewhat different in the solid than in the free atom, and this "renormalized atom" (*52*) effect tends to decrease U for increasing covalency. Second, also in the larger band gap materials the charge-transfer screening is not completely quenched. As pointed out by Herring (*53*), the screened U in metals is determined by the reaction $2E(d^ns) \rightarrow E(d^{n-1}) + E(d^{n-1}s^2)$, where the atom stays locally charge neutral. If a gap opens up in the charge excitation spectrum, the screening length will increase and this very efficient screening will get frustrated. However, the question is how fast this will go and, in fact, Gunnarsson *et al.* show that the metallic screening is still dominating in the semiconductor CdTe (*50*). In the most ionic system studied (Mn in ZnO), the charge compensation on the Mn site is only 20%; however, in addition there is a substantial charge transfer to the nearest neighbor ligand (*51*). This charge transfer screening can certainly account for the additional screening we needed.

Cation Systematics

The point we want to make here is that this classical modeling makes sense if one is interested in trends. Comparing compounds with the same anion it is expected that the changes in the solid state "corrections" will depend in first order on changes in the interatomic distances and the crystal structure. Our prime interest is in the late 3d compounds (MnX–NiX) and we observe that the crystal structures for compounds with the same anion is either the same (MF_2 rutile; MO rocksalt; MCl_2 $CdCl_2$ structure) or simi-

lar (MBr_2, MI_2: CdI_2 structure except for $NiBr_2$ and NiI_2 ($CdCl_2$ structure)). The change in the lattice constants in these series is small. The interatomic distances follow closely the ionic radii of the cations resulting in a lattice contraction of only $\approx 5\%$ in going from Mn to Ni. As a result, the p–d transfer integrals hardly change and also the ligand band widths are similar in (for instance) the series MnO–NiO as band structure calculations indicate (*54*).

It is expected that also the cation dependence of the polarization energy is moderate. For instance, according to de Boer *et al.* (*44*) the polarization energy in these materials is of the order of 3 eV and is proportional to $1/R^4$. It is found that the polarization energy is decreased by only ≈ 0.5 eV in going from NiO ($R = 2.08$ Å) to MnO ($R = 2.21$ Å), which in first instance can be neglected. Also the renormalized atom and charge transfer type corrections, dependences on the atomic Wigner Seitz sphere radii, and the magnitude of Δ_{it}, respectively, will be roughly constant across the series. Finally, we are left with the cation dependence of the Madelung potential and the atomic ionization energies, which can be affected by our assumptions concerning the charge separation. In order to see how this works out quantitatively, we compare in Fig. 6 the trends derived from the fully ionic and the ionic + 4s scenarios for the TM oxides. The ionization energies of M^+ and M^+4S and the Madelung potentials are summarized in Table I, and we used the NiO data to fix the absolute magnitude of the parameters. Surprisingly, *the trends in the parameters depend only weakly on our assumptions*. Rather arbitrarily, we use the average (drawn lines in the figure) in the remainder.

The observed trends are easily understood. With respect to U an overall decrease is noticed in going from the right to the left of the 3d series because of the increase in the radial extent of the 3d orbitals. We note that the U for Cu in Cu oxides is underestimated in our approach (*57*). Although part of this can be traced back to the strong tetragonal distortion in Cu compounds, which tends to frustrate the screening (*55*), most of this difference is because the U value for the high Tc's is for the low spin state Cu^{3+} (d^8) which is 3.5 eV larger than that for the high spin state assumed above. Near the middle of the series strong irregularities are noticed. Because of the exchange stabilization of the half-filled shell, the U_{eff} peaks strongly at Mn while at Fe, and also Cr, this quantity is small because of the exchange stabilization of the ionization state of Fe^{2+} and the affinity state of Cr^{2+} (d^5). This effect has recently been discussed by van der Marel *et al.* (*56*) for magnetic impurities in metals. In the absence of a crystal field splitting U can be written in terms of the F^0 Slater integral and two positive quantities $J = 1/14\ (F^2 + F^4)$ and $C = 1/14\ [(9/7)F^2 - (5/7)F^4]$ where F^2 and F^4 are the higher order multipole Slater integrals. These can also be written in terms of the Racah parameters using $A = F^0 - (1/9)F^4$, $B = (1/49)F^2 - (5/441)F^4$, $C = (35/441)F^4$. Using this van der Marel *et al.* showed that

$$U = F^0 + 4J \text{ for } d^5,$$

$$U = F^0 - J - C \text{ for } d^1, d^4, d^6, d^9, \text{ and}$$

$$U = F^0 - J + C \text{ for } d^2, d^3, d^7, d^8, \quad (10)$$

where the Hund's rule ground state is used in each case. It is this trend which is evident in Table 1 and Fig. 6.

With respect to Δ it is seen that it increases from the right to the left, as expected, while again near Mn irregularities are noticed. Mn has a large Δ because of the exchange stabilization of the half-filled d^5 ground state compared to $d^6\underline{L}$. At Cr the d^{n+1} configuration corresponds with d^5, giving rise to a sharp drop of Δ for this ion.

Before we can use these numbers, a final correction remains to be made: crystal field effects are quite strong in TMCs, and one should define the Δs and U_{eff}s with respect

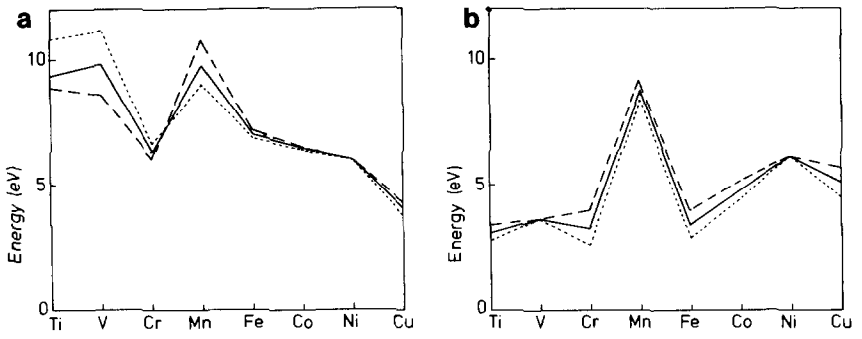

FIG. 6. (a) Charge transfer energies for the oxides and chlorides obtained from atomic ionization potentials. The dotted line corresponds to Δ^i, dashed line to Δ^s, and the solid line is the average (Δ). (b) Effective Us for the oxides and chlorides. Dotted line corresponds to U^i, dashed line to U^s, and solid line is the average (U).

TABLE I

IONIZATION POTENTIALS OF THE MONOVALENT TM IONS, MADELUNG POTENTIALS, AND CHARGE TRANSFER ENERGIES FOR THE DIVALENT 3*d* TRANSITION METAL OXIDES

(*a*)	E_I^s(at)	E_I^i(at)	$2E_{Mad}$ ($M^{2+}O^{2-}$)	$\bar{\Delta}$	$\tilde{\Delta}$	Δ_0	Δ_{Cr}	Δ_{Cr}
Cu	10.55	20.29	48.?	4.?	Δ_0	4.	Δ_0	4.0
Ni	8.76	18.15	47.98	(6.)	$\Delta_0 + 8B$	4.92	$\Delta_0 + 8B$	6.0
Co	7.90	17.05	47.26	6.5	$\Delta_0 + 7B$	5.53	$\Delta_0 - 8B - J(^4T_1)$	5.4
Fe	6.94	15.87	46.60	7.	$\Delta_0 + 6B$	6.21	$\Delta_0 + J(^4J_1) + 21B - 20$ Dq	6.1
Mn	2.77	13.82	45.63	9.9	$\Delta_0 + 14B$	8.23	$\Delta_0 - 10$ Dq $+ 14B$	8.9
Cr	8.27	16.49	47.?	6.3?	$\Delta_0 - 14B$	7.74	$\Delta_0 - 14B$	6.3
V	6.81	14.20	49.18	9.9	$\Delta_0 - 6B$	10.47	$\Delta_0 - 6B$	9.9
Ti	6.01	13.51	48.14	9.4	$\Delta_0 - 7B$	10.02	$\Delta_0 + 30$ Dq $- 15B - J(^3T^1)$	8.3
(*b*)	U^s(at)	U^i(at)	U	B	C	$\tilde{U}$	$A-$	U_{Cr}	U_{Cr}
Cu	14.66	16.33	5.10	0.1535	0.5776	$A - 8B$	6.33	$A - 8B$	5.1
Ni	15.09	17.95	6.13	0.1345	0.5999	$A + B$	(6.00)	$A + J(^4T_1) + 16B$	7.3
Co	14.12	16.20	4.77	0.1382	0.5413	$A + B$	5.02	$A - 29B - 2J(^4T_1) + 20$ Dq	4.9
Fe	12.94	14.66	3.41	0.1312	0.4836	$A - 8B$	4.46	$A + 7B + J(^4T_1) - 10$ Dq	3.5
Mn	18.11	20.20	8.76	0.1190	0.4122	$A + 28B$	5.43	$A + 28B - 10$ Dq	7.8
Cr	12.91	14.41	3.27	0.1029	0.4253	$A - 8B$	4.09	$A - 8B$	3.3
V	12.53	15.51	3.63	0.095	0.3540	$A + B$	3.54	$A + 9B + J(^3T_1) - 30$ Dq	4.8
Ti	12.36	14.65	3.11	0.089	0.3260	$A + B$	3.02	$A - 15B - 2J(^3J_1) + 80$ Dq	2.9

[a] The superscripts *s* and *i* refer to the two approximations in the text with and without an extra 4*s* electron, respectively. $\bar{\Delta}$ is the average charge transfer energy based on $\bar{\Delta} = 6.0$ eV for NiO which is experimentally determined. $J(^4T_1) = (-15B + 30\text{ Dq} - \frac{1}{2}((9B + 10\text{ Dq})^2 + 144B^2)^{\frac{1}{2}}$ and $J(^3T_1) = (-B + 90\text{ Dq} - \frac{1}{2}((9B + 10\text{ Dq})^2 + 144B^2)^{\frac{1}{2}}$. All energies are in electron volts.

[b] Same as in footnote *a* but now for the *d*–*d* Coulomb interaction U. $\tilde{U}$ and $\tilde{A}$ are based on the experimental values of 6.13 and 6.0 respectively for NiO.

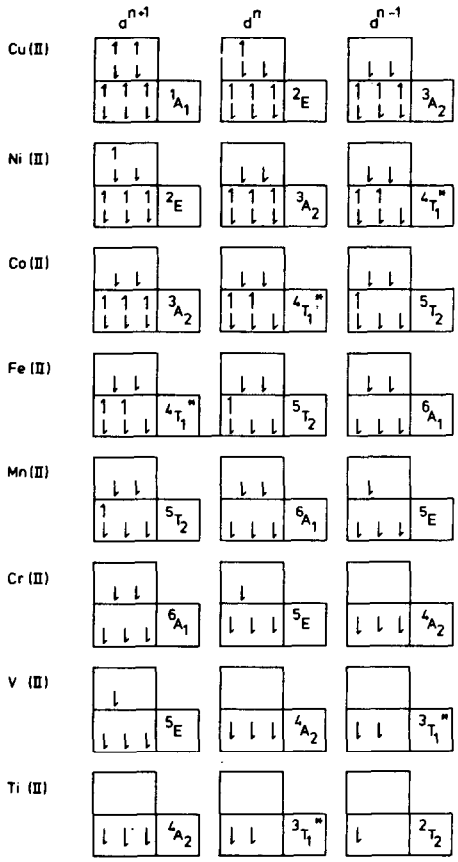

FIG. 7. The lowest energy d^{n+1}, d^n, and d^{n-1} states in O_h. The strong field ground states are indicated for $d^7(^4T_1)$ and $d^2(^3T_1)$. * indicates twofold representations.

to the strong field configurations, indicated in Fig. 7. The corrections to be applied to these quantities are also summarized in Table I, and using 10 Dq = 1 eV for the oxides one finds some minor corrections compared to the quasi-atomic case as shown in Fig. 8. First, we notice that compared to Ni the charge transfer energy is lowered by $\approx$ 10 Dq for Co to Mn. This can be understood from Fig. 7 where it is seen that in the latter an extra t_{2g} electron is present in the d^{n+1} state compared to the d^n state, thereby decreasing Δ with $\approx$ 10 Dq. For Fe and Co the crystal field splitting does not affect U because two and four respectively t_{2g} holes are present both in the "initial" (d^n) and "final" (d^{n+1}, d^{n-1}) stateof the process for which U is determined. For Ni the crystal field increases U_{Cr} because of the t_{2g} hole present in the d^7 state and for Mn U_{Cr} is decreased by the extra t_{2g} hole in the d^6 state.

We note again that we are in error for Cu(II) compounds because we assumed octahedral coordination instead of square planar and the appropriate U mostly used is the one corresponding to the low spin Cu III state. This is a state with two holes in a $x^2 - y^2$ orbital. The corresponding U is $A + 4B + 3C$ which has been experimentally determined in CuO to be 8.8 eV (*57*).

Finally, we notice that the U_{eff}s and Δs determined in this way are in general not the ones determining the superexchange (*19*). The intermediate d^{n-1} states entering the perturbation theory for the superexchange have spin $S - 1/2$, instead of the $S + 1/2$ for divalent Fe, Co, Ni, and Cu. The latter is used to determine the U as given by Eq. (2).

Anion Systematics

We assume that the cation dependence of the parameters is not changed in going to a

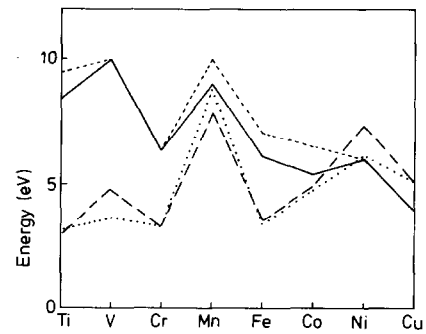

FIG. 8. The charge transfer energy (Δ_{Cr}, solid line) and U_{eff} (U_{Cr}, dashed line) including the electrostatic crystal field contributions compared to the quasi-atomic Δ and U (dashed line and dotted line, respectively).

different anion. From our discussion it may be clear that it is very hard to arrive at reliable parameters upon changing the ligands by using simple model considerations. We therefore use purely empirical estimates for these. Ni compounds have been investigated most thoroughly, and we use these data to determine the trends as a function of anion.

Considering the charge transfer energy it is expected that this quantity will increase for increasing electronegativity of the anion. This is confirmed by core-XPS and XAS experiments from which we found that $\Delta(NiI_2) < \Delta(NiBr_2) < \Delta(NiCl_2) \approx \Delta(NiO) < \Delta(NiF_2)$ (*58, 59*). These results are not very sensitive to the actual magnitude of Δ because the energetics in the core ionized state is determined by the difference between Δ and the core $3d$ Coulomb interaction. They confirm however that the conductivity gap in NiO_2, $NiBr_2$, and $NiCl_2$ is of charge-transfer character. In this regime $E_{gap} \alpha \Delta$ and the gap magnitudes determined by recent photoconductivity measurements (*13*) ($E_{gap}(NiCl_2)$ = 4.7 eV, $E_{gap}(NiBr_2)$ = 3.5 eV, $E_{gap}(NiI_2)$ = 1.8 eV) follow closely the trends in Δ as determined by core spectroscopies. The charge transfer energies can be estimated from $E_{gap} = \Delta - 1/2W + \delta^{N+1} + \delta^{N-1} - 2\delta^N$ (*23*). Taking for the hybridization correction $\delta^{N+1} + \delta^{N-1} - 2\delta^N \approx 0.5$ eV and a bandwidth W = 4 eV (see Refs. (*61* and *29*)) we end up with estimates for Δ shown in Table II. For NiO we use the Δ value determined from the photoemission/inverse photoemission spectra and $\Delta(NiF_2)$ is estimated by extrapolating from $\Delta(NiCl_2)$ using the trend predicted by core spectroscopy.

The anion dependence of U can be determined by analyzing the photoemission and inverse photoemission spectra, and the latter have not yet been obtained except for NiO. However, under the assumption that the lowest affinity state is nearly pure d^9 in the Ni compounds only the conductivity gap magnitude is needed together with the photoemission spectra as Hüfner pointed out (*62*). Assuming that the photoemission satellites correspond with d^7 states, the suggestion from Hüfner's data would be that U increases severely in going from $NiBr_2$ to NiF_2. This is a quite dangerous procedure because of the d^9 to photoemission-satellite splitting contains hybridization corrections. For instance, according to Hüfner's procedure the U would be considerably smaller in $NiCl_2$ compared to NiO. However, these changes can be for the most part explained by a moderate decrease in the transfer integrals in going from NiO to $NiCl_2$ while keeping Δ and U the same.

In any case U is expected to decrease in going from the fluorides to the iodides because of the decreasing band gaps and the increasing anion polarizabilities. The analysis of the core spectra of the Ni-dihalides (*58*) and Cu-dihalides (*63*) suggest however that these changes are rather moderate. In Ref. (*58*) we rationalized this behavior by considering the polarization energies. We found there that the increase of the anion polarizabilities in going from the fluorides to the iodides is largely compensated by the increase of the interatomic distances, leaving only a small net increase of the polarization energies ($E_{pol}(NiI_2)$ = 2.9 eV, $E_{pol}(NiBr_2)$ = 2.7 eV, $E_{pol}(NiCl_2) = E_{pol}(NiF_2)$ = 2.4 eV). To arrive at a first order estimate for the anion dependence of U_{Cr} we assume

TABLE II

ESTIMATES FOR Δ_{Cr} AND U_{Cr} AND THE ITINERANT BAND GAP ($\Delta_{it} - 1/2W$) FOR THE DIVALENT Ni COMPOUNDS

	S	I	Br	Cl	O	F
U_{Cr}	3.3	6.3	6.7	7.3	7.3	7.3
Δ_{Cr}	1.	3.	5.	6.	6.	9.
$\Delta_{it} - 1/2W$	5.	6.	7.	8.	11.	15.

Note. All energies in electronvolts.

that the reduction of U follows the trend in these polarization energies. Assuming that $U_{Cr}(NiCl_2) \approx U_{Cr}(NiO)$ we find the Us as summarized in Table II.

In order to account completely for the electronic structure of the 3*d* compounds also the gap separating the itinerant states (Δ_{it}) has to be determined. It is expected that, as for Δ, this gap decreased with decreasing anion electronegatives. Folkerts and Haas (*64*) showed that the structure of the γ excitons (ligand p hole-conduction band electron) can be used to determine the location of the p–s transition in the optical spectra. Estimates for the itinerant gaps obtained by these authors for NiI_2, $NiBr_2$, and $NiCl_2$ are included in Table II and these numbers follow the expected trend. Regarding the cation dependence of this gap, band structure calculation (*54, 30, 45*) indicates that it is roughly constant in the series MnX–NiX and this is confirmed by the optical measurements (*64*).

The γ excitons in the optical spectrum of NiO have not yet been analyzed. It is, however, tempting to assign the upturn seen at $\approx$ 11 eV in the optical spectrum of NiO (*65*) to these transitions. Also the $L_{2,3}$ XAS spectra of the Ni compounds can be used to determine trends in Δ_{it} as we showed in Ref. (*59*) and these data confirm that $\Delta_{it}(NiO)$ is about 3 eV larger than $\Delta_{it}(NiCl_2)$. We have not found optical data over a sufficient range of NiF_2 in the literature. We therefore have to rely on the XAS data which indicate a very large Δ_{it} in this material ($\approx$ 17 eV). This number seems to be unphysically large and optical measurements can shed further light on this matter.

For illustrative purposes we included also parameters typical for metallic NiS. The small satellite in the core-XPS spectrum of NiS (*60*) suggests that U has dropped down to a typical metallic value ($\overline{A} \approx 3$ eV). Because of the large p–d hybridization and the importance of d–d dispersional width, it is difficult to decide what to take for Δ and we used a value for this quantity which reproduces in the impurity picture the d count expected from the magnetic moment in the antiferromagnetic phase ($<nd> \approx d^{8.5}$). The itinerant gap can be estimated from the photoemission inverse spectra of this material (*24*).

The Nature of the Single Particle and Electron-Hole Excitation Spectra

Having determined the important parameters, we now discuss how the nature of the excitation spectra depends on cations and anions. We first focus on the cation dependence. Using parameters, representative for chlorides, we sketch in Fig. 9 the single particle spectra, following the procedure outlined in the Introduction. If one places the bottom of the 4*s*-like conduction band at $\approx$ 3 eV higher energy, one obtains our prediction for the oxides. At least for the heavier members of the series, there is not much variation in the unoccupied states. The conduction band onset is well above the upper Hubbard band, and at low energies the electrons should be well described by carriers moving in the d^{n+1} Hubbard band. In the occupied DOS there is more action in going from Cu to Fe. The charge transfer energy is only weakly cation dependent, but U decreases strongly in this series. Therefore, the most extreme charge transfer materials are the cuprates, at least in square planar coordination and in going to Fe(II), the lower Hubbard band crosses the ligand p band, and we predict that $FeCl_2$ or FeO are in fact "classical" Mott–Hubbard insulators. Equally, upon hole doping, the chance to find low spin "TM(III)" states is largest in the cuprates, while in Fe(II) compounds high spin carriers are more likely, according to the Eskes–Sawatzky diagram (*36*).

At the beginning of the series, this trend is reversed and the action is expected to

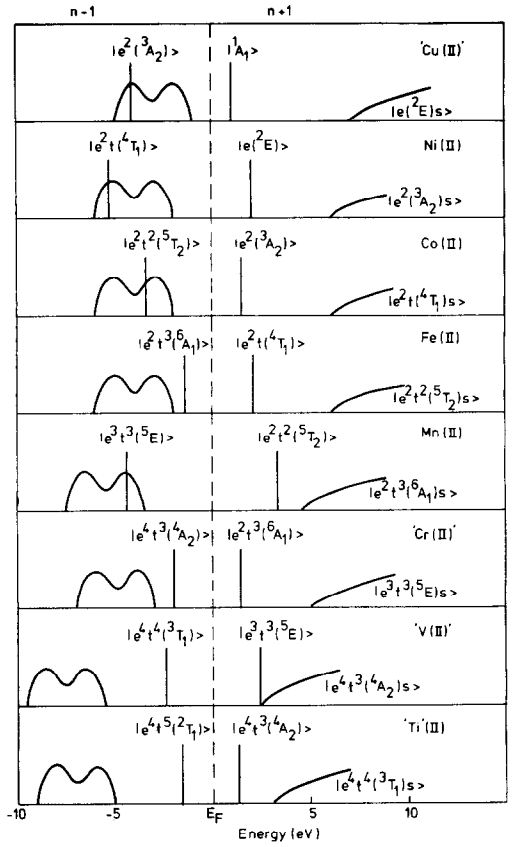

FIG. 9. The d^{n-1} and d^{n+1} states relative to the ligand p-band ($d^n\underline{L}$) and the conduction band ($d^n s$). These diagrams are obtained using parameters characteristic for the transition metal dichlorides.

occur above the Fermi energy. Here the holes go into the lower Hubbard band, while the s-upper Hubbard band mixing is much stronger. The light counterpart of Fe(II) is Cr(II). The s band is here at relatively high energy because of the exchange stabilization of the high spin $d(5)$ upper Hubbard band, while in Fe the lower Hubbard band is exchange stabilized. Because in Mn(II) the $d(5)$ ground state is exchange stabilized, compounds of this element stay alone in the series. Both the upper and lower Hubbard bands are relatively unfavorable and here one expects the strongest admixing of non-d states both at the bottom of the conduction and top of the valence band.

Apparently it makes sense to distinguish four families of TM(II) ions. Clearly, the early $3d$'s stand apart. Next, we have the right end of the series (Cu(II) and Ni(II)) where we expect to find in about all cases charge-transfer insulators. The neighbors of Mn (Fe(II) and Cr(II)) are quite similar and these are the candidates for having the d–d gaps similar to the early $3d$'s. Finally, Mn(II) stands alone because of its exchange-stabilized ground state.

In Fig. 10 we show the behavior of the excitation energies of direct relevance to the nature of the band gap for these four cation families as a function of the anion. These energies are the charge transfer energy Δ_{Cr} (ligand p–d gap), $U_{Cr}(d$–d gap), $\Delta_{it} - 1/2W$ (ligand p-conduction band–s gap), and $U_{Cr} - \Delta_{Cr} + \Delta_{it}$ (d–s gap). The conductivity gap of Ni compounds is always dominated by charge-transfer excitations. The d–d excitations will become, however, more important if the ionicity increases. Up to $NiCl_2$ charge-transfer insulators are expected, NiO is on the boundary of the intermediate regime while in NiF_2 the d–d excitations probably are quite important.

In going from Ni to Fe compounds the role of the d–d and charge transfer excitations has been reversed. The more ionic Fe compounds are expected to be Mott–Hubbard-like while for increasing covalency the charge transfer excitations will become more important. As a consequence, we predict that the conductivity gap will decrease in going from Ni to Fe compounds if the anion electronegativity is large (O, Cl, F) while the gap will stay roughly constant for the iodides. We note that FeS is predicted to be metallic and that the U drops below zero. This attractive d–d interaction is not an artefact of the ionic model. It is also found in the metallic screening models and it is due to the large screening of the monopole part of the d–d

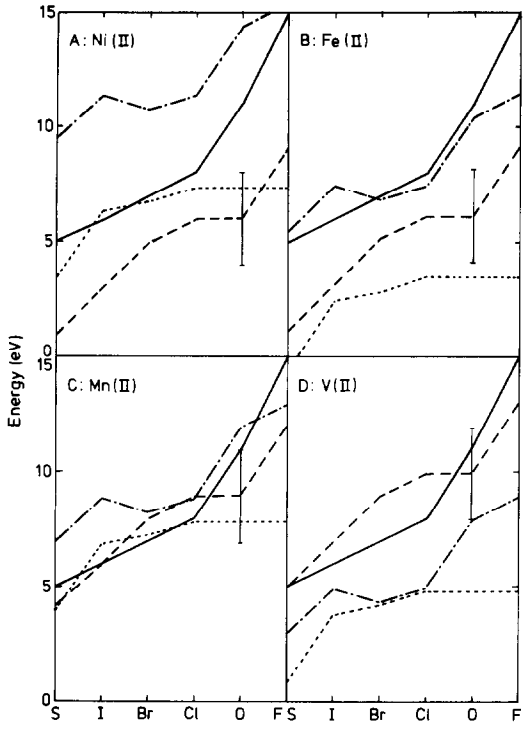

FIG. 10. The important electronic excitation energies in the 3*d* compounds as a function of the anions for the four archetypical 3*d* ions. Indicated are the charge transfer (*p*–*d* gap) energy (Δ_{Cr}, dashed line), the itinerant gap magnitude ($\Delta_{it} - 1/2W$, solid line), the *d*–*d* gap magnitude (U_{Cr}, dotted line), and the *d*–*s* gap magnitude ($U - \Delta_{Cr} + \Delta_{it}$, dashed–dotted line). Also the ligand *p* bandwidth is indicated (vertical bar).

Coulomb interaction while the exchange interactions are screened much less, as discussed by van der Marel (*56*).

Turning to Mn compounds the significant finding is that at least up to $MnCl_2$ all the excitations are at comparable energy. As a first consequence, it is now necessary to account also for the itinerant conduction band states. The d^6 state will mix strongly with the d^5s band, resulting in rather low mass electrons and also the itinerant (*p*–*s*) excitations are close to the conductivity threshold. We expect that in the Mn compounds the hole and electron mobilities are similar while in Ni compounds the hole mobility will be usually much larger than the electron mobility. It would be interesting to see if this would have consequences for the transport in these systems.

A second observation is that the charge-transfer energy in Mn compounds is much larger than in the heavy 3*d* compounds. We argued that the charge transfer energy is the limiting factor for the band gap magnitude of the compounds of Fe–Cu with relatively electropositive anions (S,I). Because of the sudden increase of the charge transfer energy, the gaps of the sulfides and divalent iodides will increase substantially at Mn. We see that even MnS is predicted to be an insulator, consistent with the finding that this is the only nonmetallic sulfide (see Wilson (*4*)). The actual band gap of MnS is $\approx$ 4 eV (*66*) which compares well with the gap we find for $MnI_2 \approx 4$ eV, in agreement with the experiment (*67*). These should be comparable because of the comparable electronegativity of these anions. We note that the gap determined from the figure for MnS ($\approx$2 eV) as based on metallic NiS as a reference is considerably smaller.

As expected, in the early 3*d* compounds the *d*–*s* and *d*–*d* excitations are found to be most important. According to our picture the *d*–*s* excitations are still at rather high energy. This is not consistent with the results of band structure calculations where it is found that for the oxides the *s* and *d* states are strongly mixed (*45, 54*). In impurity language, the insulator to metal transition in going from MnO to VO would be driven by the crossing of the Fermi level by the 4*s* band, as suggested earlier by Koiller and Falicov (*15*). This can be only part of the story. In going from Cr(II) to V(II) the e_g subshell becomes empty which drives a lattice contraction (see e.g., Ref. (4)) which in turn increases the *d*–*d* bandwidth and the *p*–*d* and *s*–*d* mixing and strongly reduces the charge transfer energy.

TABLE III

THEORETICAL ESTIMATES FOR THE p–d (Δ'_{Cr}) AND THE d–s ($U'_{Cr} - \Delta'_{Cr} + \Delta'_{it}$) THRESHOLDS COMPARED TO THE EXPERIMENTAL OPTICAL GAPS OF $3d$ IMPURITIES IN INSULATORS

	Ni^{2+}	Co^{2+}	Fe^{2+}	Mn^{2+}	Cr^{2+}	V^{2+}
$KMgF_3 : M^{2+}$						
Δ'_{Cr}	(8.4)	7.8	8.5	13.3	8.7	12.3
$U'_{Cr} - \Delta'_{Cr} + \Delta'_{it}$	10.	8.2	(6.1)	7.6	5.7	3.6
Experiment	8.4	7.8	6.1	7.5	5.7	4.6
$LiCl : M^{2+}$						
Δ'_{Cr}	(4.8)	4.2	4.9	7.8	5.1	8.7
$U'_{Cr} - \Delta'_{Cr} + \Delta'_{it}$	10.6	8.8	6.8	8.2	6.3	4.2
Experiment	4.8	4.8	5.4	6.8	4.8	4.

Note. All energies in electronvolts.

Optical Spectra

In contrast to PES/BIS, several optical studies exist focusing on the trends in the $3d$ series. Although somewhat less direct, we will show that these data can be used to confirm the picture presented in the last section. Let us first consider some impurity systems, before we turn to the more complicated situation in the compounds.

In $3d$ impurity systems, only the $p \rightarrow d$ and the $d \rightarrow s$ transition are of relevance. The onsets of these transitions are according to our parametrization at Δ'_{Cr} and $U_{Cr} - \Delta'_{Cr} + \Delta'_{it}$, absorbing the ligand valence bandwidth in the parameters ($\Delta'_{Cr} = \Delta_{Cr} - 1/2W$, $\Delta'_{it} = \Delta_{it} - 1/2W$). Therefore, both the trends in Δ and U can be checked if these edges can be identified. In Table III, we compare the optical thresholds of $3d$ impurities in KMgF3 (*39*) and LiCl (*40*) with our estimates. We used for the bulk bandgaps Δ'_{it}(KMgF3) = 10 eV (*39*) and Δ'_{it}(LiCl) = 8.1 eV (*41*), respectively. We fix the absolute values for Δ'_{Cr} using the Ni thresholds because in both systems these are obviously related to charge transfer transitions (*39, 40*). Assuming that the threshold in KMg F3 : Fe corresponds to a d–s transition we fix the Us in the KMgF3 series and because it is difficult to determine U directly from the data, we take the TM-chloride Us for the TM impurities in the LiCl series. Our estimates for the optical thresholds are summarized in Table III. The trends in the data are well reproduced and the quantitative agreement is, especially for the KMgF3 series, surprisingly good. The trends are clear, in the ionic KMgF3 systems C–T thresholds are only realized in Ni and Co. From Fe onwards, the gaps are of d–s character and in this series we notice the special status of Mn. LiCl systems are more covalent, and up to Cr C–T gaps are found.

Apart from the p–s, p–d, and d–s transitions, also the intersite d–d (or "intervalence" (*42*)) transitions $2TM^{2+} \rightarrow TM^{+} + TM^{3+}$ might be seen in optical spectra. The main qualitative features of such a transition can be extracted from a simple model. The direct interatomic dipole matrix elements are very small, and the intensity of these transitions should be directly related to covalency effects.

Consider a three center model with one central L ion and two surrounding TM ions, as used in superexchange calculations. To keep things simple we assume that only two holes are present in the cluster. Neglecting spin the following states have to be taken into account for the ground state

$$|dd; g> = |d_L d_R> \tag{11}$$

$$|dL; g> = 1/\sqrt{2}\,(|d_L L> + |L d_R>) \tag{12}$$

$$|d^2; g> = 1/\sqrt{2}\,(|d_L^2> + |d_R^2>) \tag{13}$$

$$|L^2; g> = |L^2>, \tag{14}$$

where d_L denotes a hole in the d shell of the left cation, d_R a d hole on the right cation, and L a hole in the p shell of the anion. These states are at energy $(E|dd; g>) = 0.$, $E(|d\underline{L}; g>) = \Delta$, $E(|d^2; g>) = U$, and $E(|L^2; g>) = 2\Delta$, and a hybridization matrix element is assumed $<d_{L,R}|H|L> = V$. The ground state of the cluster is a linear combination of these states and for $U, \Delta \gg V$ the

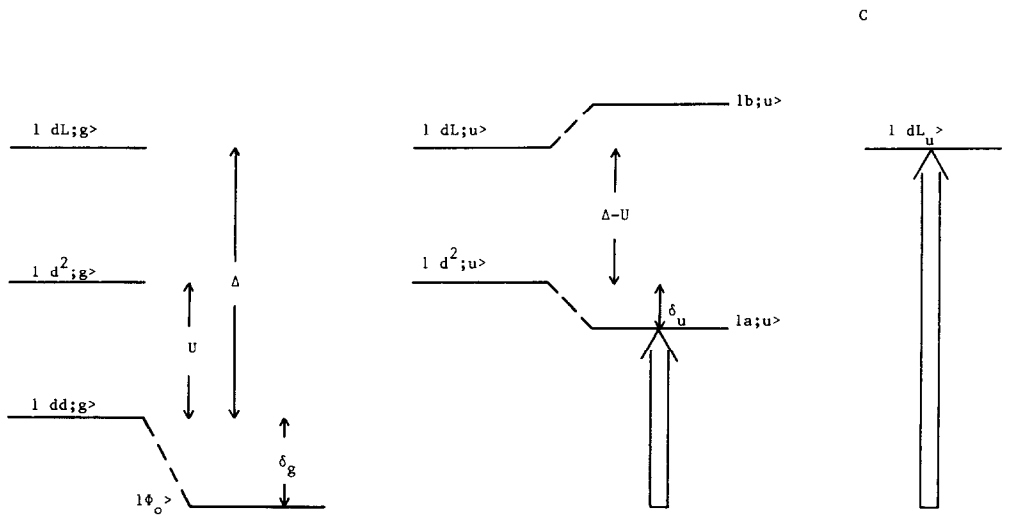

FIG. 11. Energy diagrams for the three center model ($U < \Delta$). In A the states are indicated contributing to the ground state ($|\phi_0>$) of the cluster. In B the states reached in the optical transition are indicated and the optical gap magnitude is indicated by the arrow. C is as B but now for a single cation cluster.

ground state hybridization shift is given by $\delta_g \approx -2V^2/\Delta$.

With respect to the inversion center of the cluster (the anion) the states in Eqs. (*11–14*) are gerade. According to the dipole selection rules parity has to be changed in the optical transition. The final states reached in optical spectroscopy are thus linear combinations of the ungerade states

$$|dL; u> \; 1/\sqrt{2}\,(|d_L L> - |L d_R>) \quad (15)$$

$$|d^2; u> \; = \; 1/\sqrt{2}\,(|d_L^2> - |d_R^2>), \quad (16)$$

which are located at $E(|dL; u>) = \Delta$ and $E(|d^2; u>) = U$ (see Fig. 11). These states are also hybridized ($<dL; u|H|d^2; u> = V$).

The ungerade eigenstates can then be written as

$$|a; u> \; = \cos\theta|d^2; u> \; + \; \sin\theta|dL; u> \quad (17)$$

$$|b; u> \; = \sin\theta|d^2; u> \; - \; \cos\theta|dL; u>. \quad (18)$$

The large (d–L) dipole matrix element is between the $|dd; g>$ and the $|dL; u>$ state:

$$T = <dd; g|\vec{r}|dL; u>. \quad (19)$$

According to this model, the optical absorption spectrum would consist of two lines with intensity ratio $I_a/I_b = \tan^2\theta$ where θ depends on Δ-U and V.

Considering now the Mott–Hubbard case where $\Delta > U$, the lowest state is largely of $d^2; u>$ character. The optical edge is located at $U + \delta_u - \delta_g$ (see Fig. 11) and for $\Delta - U \gg V$ we find for the edge position and intensity

$$E_{gap}(\Delta > U) \simeq U + \frac{V^2}{\Delta - U}\left(1 - 2\frac{U}{\Delta}\right) \quad (20)$$

$$I_{gap}(\Delta > U) \simeq \frac{V^2}{(\Delta - U)^2} \cdot t_{pd}^2. \quad (21)$$

Thus the intensity of the intervalence transitions is proportional to the weight of the $d^{n+1}\underline{L}$ configurations, which are admixed in the $d^{n-1}d^{n+1}$ band because of covalency.

In Fig. 12 we show our expectation for the $TMCl_2$ optical spectra, derived from the

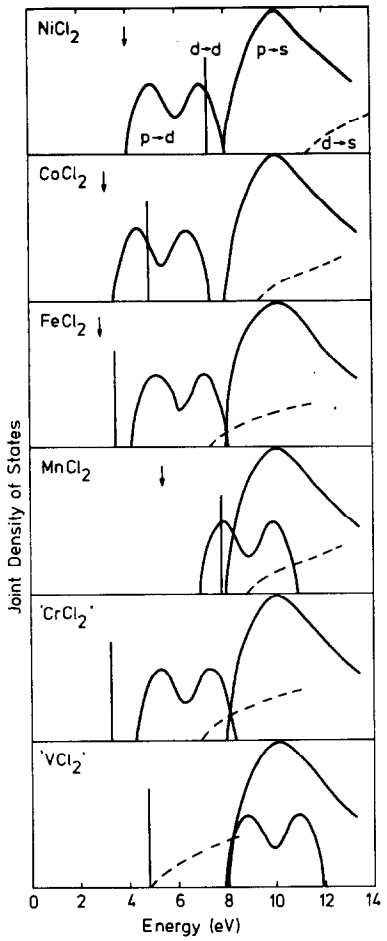

FIG. 12. The location of the p–d, d–d, p–s, and d–s lowest energy bands in the optical spectra of the divalent transition metal compounds according to our theory. The arrows indicate the experimental optical gaps.

parameters of the last section. Considering the series $NiCl_2$ to $FeCl_2$, it is seen that the p–d and d–s transitions barely change. The d–s transitions come down. However, they do not approach the optical threshold. As expected, the action is in the intervalence d–d transition which cross the p–d continuum in going from $NiCl_2$ to $FeCl_2$. Accidentally, in $MnCl_2$ all the thresholds end up very close in energy, while the optical gap is here at a maximum. In Fig. 13 we show the experimental result (*41*), and the interpretation is obvious. In $NiCl_2$, we are looking at the intense p–d transitions, whose threshold is sharpened by p–d exciton formation. Going via $CoCl_2$ to $FeCl_2$, this edge is blurred and a low intensity, low energy tail develops. Clearly, these are the intervalence transitions, stealing the intensity of the higher lying p–d transitions. Finally, in $MnCl_2$ the optical gap opens up again, being the largest in the series, while the absorption is strong near threshold because the p–d excitations are again strongly mixed in this regime.

Conclusions

We have used experimental photoemission and optical data together with free atom data to determine the trends of the d–d Coulomb interactions and charge transfer energies in the $3d$ transition metal compounds. From this we conclude that the divalent Ni and Cu compounds are either charge transfer gap insulators or for the more electropositive type of anions like S, Se, and Te these would be p-type metals with holes in the anion p band. The dihalides of Cu and Ni are predicted to exhibit a gap proportional to the anion electron negativity decreasing

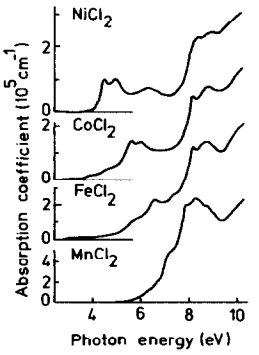

FIG. 13. Absorption spectra of the divalent transition metal chlorides according to Sakisaka, Ishii, and Sagawa (see Ref. (*68*)).

in the series F_2–Cl_2–Br_2–I_2. In contrast to this the early $3d$ divalent TM compounds (Ti, V) are Mott–Hubbard systems with a d–d gap. Divalent Fe and Cr compounds will in most cases also exhibit a d–d gap because of the very low U value caused by the effective attractive contribution due to exchange. Divalent Mn compounds stand apart because of the large stabilization of the d^5 high spin ground state. This causes both U and Δ to be anomalously large. This explains why MnS is the only nonmetallic divalent sulfide in the series.

We have also shown that the contribution of the B and C Racah parameters to U are very large resulting in considerably different U values suitable for the gap calculations as compared to the superexchange calculations. The systematics found for U, Δ, and the O $2p$–TM $4s$ band energies are used to describe optical data for both impurity doped systems and the pure compounds. Systematic trends and the nature of the absorption edges can be well described. This we believe is a strong confirmation of the systematics proposed.

Acknowledgments

This investigation was supported by the Netherlands Foundation for Chemical Research (SON) and the Foundation for Fundamental Research on matter (FOM).

References

1. J. C. Bednorz and K. A. Muller, *Z. Phys. B* **64,** 189 (1964).
2. H. J. de Boer and E. J. W. Verwey, *Proc. Phys. Soc. London A* **49,** 59 (1937).
3. F. Bloch, *Z. Phys.* **57,** 545 (1929).
4. A. H. Wilson, *Proc. R. Soc. London A* **133,** 458 (1931).
5. N. F. Mott, *Proc. Phys. Soc. Sect. A* **62,** 416 (1949).
6. J. Hubbard, *Proc. R. Soc. London A* **277,** 237 (1964); **281,** 401 (1964).
7. P. W. Anderson, *Phys. Rev.* **115,** 2 (1959).
8. J. B. Goodenough, *Phys. Rev.* **100,** 564 (1955); J. Kanamori, *J. Phys. Chem. Solids* **10,** 87 (1959).
9. M. Gutzwiller, *Phys. Rev. A* **134,** 923 (1964); *Phys. Rev. A* **137,** 1726 (1965).
10. W. F. Brinkman and T. M. Rice, *Phys. Rev. B* **132,** 4302 (1970).
11. D. B. McWhan, J. P. Remeika, T. M. Rice, W. F. Brinkman, J. Maita, and A. Menth, *Phys. Rev. Lett.* **27,** 941 (1971); *Phys. Rev. B* **5,** 2252 (1972).
12. J. A. Wilson, *Adv. Phys.* **21,** 143 (1972).
13. C. R. Ronda, G. J. Arends, and C. Haas, *Phys. Rev. B* **35,** 4038 (1987).
14. R. Merlin, T. P. Martin, A. Polian, M. Cardona, B. Andlauer, and D. Tannhauser, *J. Magn. Magn. Mater.* **9,** 83 (1978).
15. B. Koiller and L. M. Falicov, *J. Phys. C* **7,** 299 (1974).
16. D. Adler and J. Feinlieb, *Phys. Rev. B* **2,** 3112 (1970).
17. G. A. Sawatzky and J. W. Allen, *Phys. Rev. Lett.* **53,** 2239 (1984).
18. A. Fujimori, F. Minami, and S. Sugano, *Phys. Rev. B* **27,** 5225 (1984); A. Fujimori and F. Minami, *Phys. Rev. B* **30,** 957 (1984).
19. J. Zaanen and G. A. Sawatzky, *Canad. J. Phys.* **65,** 1262 (1987).
20. G. A. Sawatzky, *Int. J. Mod. Phys. B* **1,** 779 (1988).
21. J. A. Yarmoff, D. R. Clarke, W. Drube, U. A. Karsson, A. Taleb-Ibrahimi, and F. J. Himpsel, *Phys. Rev. B* **36,** 3967 (1987).
22. P. Kuiper, G. Kruizinga, J. Ghijsen, G. A. Sawatzky, and H. Verweij, *Phys. Rev. Lett.* **62,** 221 (1989).
23. J. Zaanen, G. A. Sawatzky, and J. W. Allen, *Phys. Rev. Lett.* **55,** 418 (1985).
24. J. Zaanen, G. A. Sawatzky, and J. W. Allen, *J. Magn. Magn. Mater.* **54–57,** 607 (1986).
25. G. A. Sawatzky, *in* "Auger Spectroscopy and Electronic Structure" (G. Cubiotti, G. Mondio, and K. Wandelt, Eds.), Vol. 18, p. 127, Springer-Verlag, New York/Berlin (1989).
26. S. Sugano, Y. Tanabe, and H. Kamimura, "Multiplets of Transition Metal Ions in Crystals," Academic Press, New York (1970).
27. Y. Tanabe and S. Sugano, *J. Phys. Soc. Japan* **9,** 767 (1954).
28. J. C. W. Folmer and F. Jellinek, *J. Less-Common Met.* **76,** 153 (1980).
29. A. M. Olés and J. Zaanen, *Phys. Rev. B* **39,** 9175 (1989); C. A. Balseiro, M. Avignon, A. G. Rojo, and B. Alascio, *Phys. Rev. Lett.* **62,** 2624 (1989).
30. T. Oguchi, K. Terakura, and A. R. Williams, *Phys. Rev. B* **28,** 6443 (1983); **30,** 4734 (1984).
31. J. Zaanen, Thesis, Groningen (1986).
32. J. F. Lang, Y. Baer, and P. A. Cox, *J. Phys. F* **11,** 221 (1981).
33. W.-D. Schneider and Y. Baer, *in* "Narrow Band Phenomena—Influence of Electrons with Both Band and Localized Character" (Fuggle, Sa-

watzky, and Allen, Eds.), Vol. 184, p. 169, Plenum, New York (1988).
34. F. D. M. HALDANE AND P. W. ANDERSON, *Phys. Rev. B* **13,** 2553 (1976).
35. H. ESKES, H. TJENG, AND G. A. SAWATZKY, *in* "Mechanisms of High Temperature Superconductivity" (H. Kamimura and A. Oshiyama, Eds.), p. 20, Springer-Verlag, New York (1989).
36. H. ESKES AND G. A. SAWATZKY, *Phys. Rev. Lett.* **61,** 1415 (1988).
37. F. C. ZHANG AND T. M. RICE, *Phys. Rev. B* **37,** 3759 (1988).
38. H. KATAYAMA-YOSHIDA AND A. ZUNGER, *Phys. Rev. Lett.* **55,** 1618 (1985).
39. J. F. SABATINI, A. E. SALWIN, AND D. A. MCCLURE, *Phys. Rev. B* **11,** 3832 (1975).
40. J. SIMONETTI AND D. A. MCCLURE, *J. Chem. Phys.* **71,** 793 (1979).
41. T. ISHII, Y. SAKISAKA, T. MATSUKAWA, S. SATO, AND T. SAGAWA, *Solid State Commun.* **13,** 281 (1973); Y. SAKISAKA, T. ISHII, AND T. SAGAWA, *J. Phys. Soc. Japan* **36,** 1365 (1974).
42. S. WITTEKOEK, T. J. A. POPMA, J. M. ROBERTSON, AND P. F. BONGERS, *Phys. Rev. B* **12,** 2777 (1975).
43. P. W. ANDERSON, *Phys. Rev.* **115,** 2 (1959); YA.M. KSENDZOV AND I. A. DRABKIN, *Sov. Phys. Solid State* **7,** 1519 (1965).
44. D. K. G. DE BOER, Thesis, University of Groningen (1983); D. K. G. DE BOER, C. HAAS, AND G. A. SAWATZKY, Phys. Rev. B **29,** 4401 (1984).
45. O. K. ANDERSEN, H. L. SKRIVER, H. NOHL, AND B. JOHANSSON, *Pure Appl. Chem.* **52,** 93 (1979).
46. P. H. DEDERICHS, S. BLÜCHEL, R. ZELLER, AND H. AKAI, *Phys. Rev. Lett.* **53,** 2512 (1984).
47. R. MONNIER, L. DEGIORGI, AND D. D. KOELING, *Phys. Rev. Lett.* **86,** 2744 (1986); J. M. WILLS AND B. R. COOPER, *Phys. Rev. B* **36,** 3809 (1987).
48. A. K. MCMAHAN, R. M. MARTIN, AND S. SATHAPY, *Phys. Rev. B* **38,** 6650 (1989).
49. M. S. HYBERTSEN, M. SCHLUTER, AND N. E. CHRISTENSEN, *Phys. Rev. B* **39,** 9028 (1989).
50. O. GUNNARSSON, A. V. POSTNIKOV, AND O. K. ANDERSEN, *Phys. Rev. B* **40,** 10407 (1989).
51. O. GUNNARSSON, O. K. ANDERSEN, O. JEPSEN, AND J. ZAANEN, *Phys. Rev. B* **39,** 1708 (1989).
52. J. G. HERBST, R. E. WATSON, AND J. W. WILKINS, *Phys. Rev. B* **13,** 1439 (1976); *Phys Rev. B* **17,** 3089 (1978).
53. C. HERRING, *in* "Magnetism" (G. T. Rado and H. Suhl, Eds.), Academic Press, New York (1966).
54. L. F. MATTHEISS, *Phys. Rev. B* **5,** 290 (1972).
55. V. ANISIMOV, UNPUBLISHED.
56. D. VAN DER MAREL, Thesis, University of Groningen (1985). D. VAN DER MAREL AND G. A. SAWATZKY, *Phys. Rev. B* **37,** 10,674 (1988). D. VAN DER MAREL, G. A. SAWATZKY, AND F. U. HILLEBRECHT, *Phys. Rev. Lett.* **53,** 206 (1984).
57. J. GHIJSEN, L. H. TJENG, H. ESKES, G. A. SAWATZKY, AND R. L. JOHNSON, *Phys. Rev. B.*, in press; H. ESKES, L. H. TJENG, AND G. A. SAWATZKY, *Phys. Rev. B* **41,** 288, 1990; J. ZAANEN, C. WESTRA, AND G. A. SAWATZKY, *Phys. Rev. B* **33,** 8060 (1986); G. A. SAWATZKY, *in* "Earlier and Recent Aspects of Superconductivity" (J. G. Bednorz and K. A. Müller, Eds.), Vol. 90, p. 345, Springer-Verlag, New York/Berlin (1990).
58. J. ZAANEN, C. WESTRA, AND G. A. SAWATZKY, *Phys. Rev. B* **33,** 8060 (1986).
59. G. VAN DER LAAN, J. ZAANEN, G. A. SAWATZKY, R. KARNATAK, AND J.-M. ESTEVA, *Phys. Rev. B* **33,** 4253 (1986).
60. A. FUJIMORI, *in* "Core Level Spectroscopies in Condensed Systems" (J. Kanamori and A. Kotani, Eds.), Springer Series 81, p. 136, (1987).
61. R. COEHOORN, Thesis, University of Groningen, 1985.
62. S. HÜFNER, *Solid State Commun.* **53,** 707 (1985).
63. G. VAN DER LAAN, C. WESTRA, C. HAAS, AND G. A. SAWATZKY, *Phys. Rev. B* **23,** 4369.
64. W. FOLKERTS AND C. HAAS, *Phys. Rev. B* **32,** 2559 (1985).
65. R. J. POWELL AND W. E. SPICER, *Phys. Rev. B* **2,** 2182 (1970).
66. D. R. HUFFMAN AND R. L. WILD, *Phys. Rev.* **156,** 989 (1967).
67. I. POLLINI, J. THOMAS, AND A. LENSELINK, *Phys. Rev. B* **30,** 2140 (1984); M. R. TUBBS, *J. Phys. Chem. Solids* **29,** 1191 (1968).